PERGAMON

International Journal of Multiphase Flow 26 (2000) 609–633

International Journal of Multiphase Flow

www.elsevier.com/locate/ijmulflow

Effect of dispersion characteristics on particle temperature in an idealized nonpremixed reacting jet

D.J. Glaze, S.H. Frankel*

School of Mechanical Engineering, Purdue University, West Lafayette, IN 47907-1288, USA

Received 11 June 1998; received in revised form 15 February 1999

Abstract

A detailed parametric study has been performed of inert particle dispersion characteristics and their effect on particle temperature in an idealized nonpremixed, reacting co-flow jet. A one-way coupled Lagrangian simulation was used, with the continuous phase solved using the Large Eddy Simulation (LES) technique. The spatial dispersion is characterized by the particle Stokes number and the injection location in both reacting and nonreacting jets. Results are consistent with those previously reported in the literature, where particles with a Stokes number near unity are preferentially-dispersed by the large-scale, coherent vortical structures of the shear layer. The heating characteristics are identified in terms of the governing nondimensional parameters for nonisothermal particulate two-phase flows. It is found that the particle temperature behavior is a strong function of the spatial dispersion behavior. For a majority of initial locations within the jet nozzle, particle heating is hindered by an enhanced spatial dispersion.

Keywords: Particle dispersion; Particle temperature; Large eddy simulation; Lagrangian simulation; Unsteady forces; Reacting flow

1. Introduction

Dispersed two-phase turbulent flows are important in a number of engineering applications, ranging from propulsion and energy conversion devices like gas turbine engines and pulverized coal furnaces, to industrial processes such as spray casting, spray cooling, and the application

* Corresponding author. Tel.: +1 765 494 1507; fax: +1 765 494 0530.
E-mail address: frankel@ecn.purdue.edu (S.H. Frankel).

0301-9322/00/$ - see front matter
PII: S0301-9322(99)00013-0

of protective coatings and paint (Shirolkar et al., 1996). The precise control and optimization of two-phase flows are of primary concern to increase the quality and efficiency of such processes, and need to be well-understood before models can be developed for accurate engineering calculations.

In early numerical simulations of dispersed two-phase flows, the turbulent gas-phase was typically solved with either Reynolds-averaged or Favre-averaged conservation equations (Faeth, 1983). Although time-averaged solutions of the carrier phase can provide good results for fundamental flows such as steady or decaying homogeneous turbulence, they typically fail to capture the behavior of more complex shear flows, such as mixing layers, jets, and boundary layers (Faeth, 1987). The experimental work of Brown and Roshko (1974) first revealed that turbulent shear flows were dominated by organized large-scale vortical structures, whose effects on particle behavior cannot be captured with time-averaged calculations.

Experimental studies have shown repeatedly that these coherent structures can control the dispersion behavior of suspended particles or droplets. For instance, Longmire and Eaton (1992) performed rigorous measurements and obtained many detailed flow visualizations of nonevaporating droplet dispersion in a round jet. Their results, as well as those of Ye et al. (1995) and Swanson and Richards (1997), show clearly that particles with Stokes numbers near unity interact strongly with the organized structures of shear layers. Experimental work has also shown the importance of these large-scale structures to dispersion and vapor transport from evaporating droplets in both nonreacting (Ye and Richards, 1996) and reacting jets (Eickmann and Richards, 1997).

These large-scale coherent structures can be simulated with several numerical techniques, including the discrete vortex method, direct numerical simulation (DNS), and large eddy simulation (LES) (Crowe et al., 1996), each of which has its own specific benefits. The discrete vortex method is popular for high Reynolds-number flows where viscous forces can be neglected, and was used by Chung and Troutt (1988) in one of the first successful numerical simulations of particle dispersion by coherent vortical structures of a jet shear layer.

While DNS is the most accurate solution method available for turbulent flows, it is also the most computationally demanding. As a result, its application is traditionally limited to fundamental flows with simple geometries, such as stationary or decaying homogeneous turbulence (e.g. Mashayek et al., 1997; Squires and Eaton, 1991). Although DNS studies exist in the literature for practical flows such as mixing layers or jets, it has typically been necessary to solve only the inviscid form of the Navier–Stokes equations to make the problem tractable. Some examples include Aggarwal et al. (1996b) who investigated particle dispersion in a planar shear layer and Uthuppan et al. (1994) who studied particle dispersion in an axisymmetric jet. More recently, Ling et al. (1998) were able to solve the full Navier–Stokes equations in a three-dimensional simulation of a particle-laden temporal mixing layer.

The LES technique has become increasingly popular for solving problems that are too expensive for DNS. However, the accuracy of LES when compared to DNS for dispersed two-phase flows should naturally be questioned, because of the removal of the small-scale turbulent fluctuations which can affect particle behavior. Several studies have been performed recently to support the use of LES, including those of Wang and Squires (1996a, b) and Uijttewaal and Oliemans (1996). They have shown that when applied to incompressible channel flow, LES is capable of providing good accuracy for a majority of the larger particle sizes.

Recently, there have been several studies applying LES to two-phase free shear flows, as in the study by Simonin et al. (1995) to gain insight into particle-turbulence statistics for second-order closure modeling. Other recent applications of LES include a three-dimensional temporally-developing particle-laden shear layer by Wang and Squires (1996c, 1998), and a study by Chen and Pereira (1996) where qualitative comparisons are made between LES and experimental results of particle dispersion patterns in a two-dimensional mixing layer. Models have also been recently developed to include the two-way coupling effects of droplet evaporation in LES (Menon and Pannala, 1997; Pannala and Menon, 1998).

All of these different simulation techniques contribute to a large body of work in the literature on particle dispersion and evaporation behavior in nearly-isothermal flows. A majority of dispersed two-phase flows in practical engineering applications, however, are nonisothermal due to droplet evaporation or combustion. Unfortunately, little has been done to investigate particle behavior in nonisothermal flows. Jaberi (1998) has performed a DNS study of particle-laden homogeneous nonisothermal turbulence in which two-way momentum and energy coupling was included, to investigate the relationships between the velocity and temperature fluctuations of the two phases. Lisin and Hetsroni (1995) studied the effect of inert particles on temperature fluctuations in high-temperature turbulent flows. Other recent studies that include the nonisothermal effects of droplet evaporation include a three-dimensional temporally-developing shear layer with evaporating droplets (Miller and Bellan, 1998; Mashayek, 1998), and evaporating droplets in a two-dimensional spatially-developing heated jet shear layer (Aggarwal et al., 1996a).

To the authors' knowledge, no LES or DNS have been reported of particle behavior in spatially-developing, reacting shear layers, even though this type of flow is found in nearly all propulsion and energy conversion devices. This type of nonisothermal flow warrants investigation since several fundamental issues exist that need to be better understood, such as droplet dispersion, heat-up, evaporation, and combustion. The goal of this paper is to provide a basic understanding of the fundamental spatial dispersion characteristics of particles in a reacting jet, as well as the coupling that can occur between this behavior and the heating characteristics of inert particles in a nonhomogeneous reacting shear flow. Droplet evaporation and combustion are neglected in the present study to isolate the thermal effects of particle–flame interactions. Since temperature is the primary driving force behind droplet evaporation and combustion, studying only thermal behavior will provide general insight into these more complex phenomena occurring inside vortical structures in a nonpremixed jet flame shear layer. Differences between the particle behavior in a reacting and nonreacting jet will also be illustrated, where applicable.

2. Simulation overview

A planar, two-dimensional, idealized co-flow jet diffusion flame is simulated in this study with the LES technique. This method is chosen because of its ability to capture the dominant unsteady motion of the turbulent flow, without the computational demands of a complete DNS. The dispersed-phase is treated in the Lagrangian sense, so that equations for particle velocity and temperature will be integrated along each discrete particle trajectory. The particles

are injected from single point-sources across the jet nozzle to isolate the effects of initial location. A dilute mixture can typically be assumed if the particle volume fraction is less than 10^{-6}, allowing a one-way coupled simulation (Elghobashi, 1994). This low particle loading is easily achieved with widely-spaced particles in single streams, as studied here. The one-way coupled simulation details are discussed in the following sections.

2.1. LES of nonpremixed jet flame

In the LES solution, the Favre-filtered compressible Navier–Stokes, species, and energy conservation equations are numerically integrated using a predictor–corrector compact finite-difference scheme that is second-order accurate in time and fourth-order accurate in space (Kennedy and Carpenter, 1994). Combustion is modeled as an idealized single-step exothermic Arrhenius-form chemical reaction of the type $F+rOx \rightarrow (1+r)P$, with hyperbolic tangent inlet profiles specified for both velocity and the scalar variables. The computational domain extends 10 jet slot widths in the transverse direction and 15 jet widths in the axial direction, and is discretized with a nonuniformly-spaced 101×75 finite-difference grid. The inlet conditions, as well as a sample of the instantaneous temperature distribution in the jet flame is seen in Fig. 1, clearly showing the nonisothermal coherent structures that will control the particle behavior. In this and all figures, variables with a $(\,)^*$ superscript denote quantities that has been nondimensionalized by the jet slot width (D), the velocity difference between the jet and the co-flow (ΔU), and the reference thermodynamic properties measured at the centerline of the fuel jet inlet. The inlet of the jet is forced axially and transversely with low-amplitude white noise, allowing each shear layer to destabilize and form vortices at the jet preferred-mode frequency (Hussain and Zaman, 1981). This value is measured to be $St_D = 0.30$ in this study,

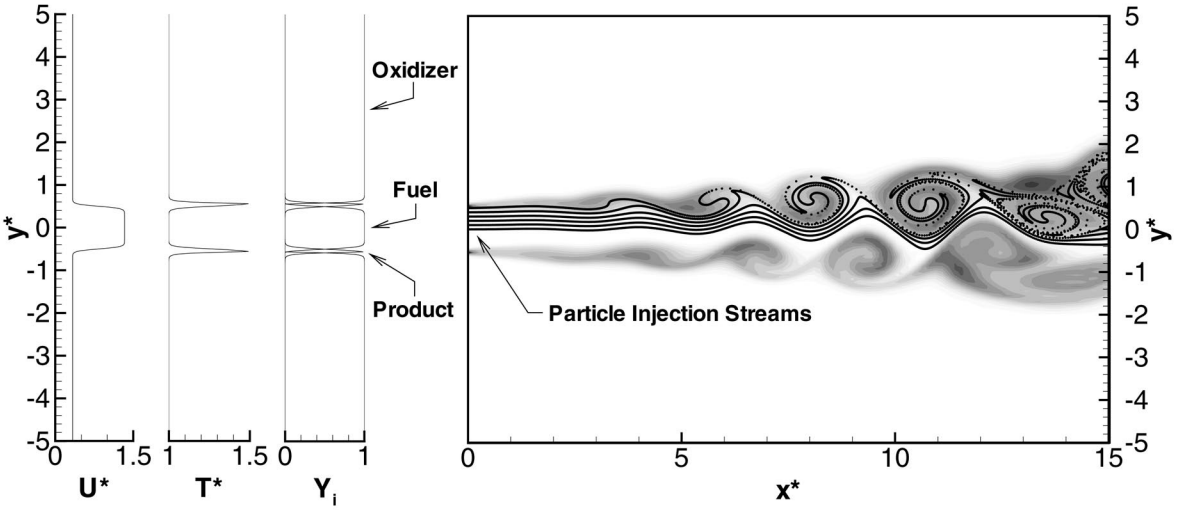

Fig. 1. Particle injection streams in a typical jet temperature distribution, showing the computational domain size and the inlet conditions.

where the Strouhal number is defined as:

$$St_D = \frac{f_p D}{\Delta U} \tag{1}$$

where f_p is the frequency (in Hz).

As a result of the Favre-filtering of the governing equations, subgrid-scale (SGS) closure models are required. For the simulations presented here, the compressible Smagorinsky SGS turbulence model is used, as well as a scale-similarity model for the filtered reaction rate. The non-dynamic formulation of the Smagorinsky model used here is certainly not the most accurate SGS turbulence model available because it tends to be overly-dissipative. The large number of simulations performed in this study forbids the use of more costly models, such as the dynamic formulation of the Smagorinsky model (Germano et al., 1991). This simple turbulence model still provides the correct qualitative structure of the jet (DesJardin, 1998), which is sufficient because of the highly-idealized qualitative nature of this study. The scale-similarity filtered reaction rate model used here is developed and tested elsewhere (DesJardin and Frankel, 1998), so details will not be repeated. These models are chosen because they are fairly inexpensive and they have been shown to provide good results in this type of application when compared to DNS.

The LES governing equations are nondimensionalized by reference thermodynamic properties at the core of the fuel jet, the jet slot width, and the velocity difference between the jet and the surrounding oxidizer co-flow. With these nondimensionalizations and a velocity ratio between the jet and co-flow of 4, a jet Reynolds number (Re) of 1000 is simulated. A jet Mach number (M) of 0.3 is used, and the molecular Prandtl (Pr), Schmidt (Sc), and Lewis (Le) numbers are fixed at 0.7, 1.0, and 1.0, respectively. In the nondimensional thermochemical transport equations, the Damköhler (Da) number, the Zeldovich (Ze) number, and the heat release parameter (Ce) are fixed at values of 10, 5, and 0.5, respectively, for the reacting jet (DesJardin and Frankel, 1998). For the nonreacting jet simulations, these parameters are all set to 0. The stoichiometric mass ratio r in the global chemical reaction is set at 13.2 to approximate acetylene–air combustion. Additionally, all thermochemical properties are assumed constant except for the dynamic viscosity, which is modeled as a function of temperature.

2.2. Lagrangian particle transport

For simplicity only inert, nonevaporating spherical particles will be simulated. This will allow a clear investigation into the fundamental thermal interactions between particles and a nonpremixed jet flame. The momentum equation for a rigid spherical particle in a nonuniform, unsteady flowfield is the well-known Basset–Boussinesq–Oseen (BBO) equation, re-derived from first principles recently by Maxey and Riley (1983). Neglecting body forces, a modified version of this equation takes the form:

$$\begin{aligned}\rho_p \mathscr{V}_p \frac{\mathrm{d}v_i}{\mathrm{d}t} &= \frac{3}{4}\frac{\bar{\rho}_f}{d_p}\mathscr{V}_p C_D \mid \tilde{u}_j - v_j \mid \left(\tilde{u}_i - v_i + \frac{1}{24}d_p^2 \frac{\partial^2 \tilde{u}_i}{\partial x_j\, \partial x_j}\right) \\ &+ \bar{\rho}_f \mathscr{V}_p \frac{D\tilde{u}_i}{Dt} + C_A \bar{\rho}_f \mathscr{V}_p \left[\frac{D\tilde{u}_i}{Dt} - \frac{\mathrm{d}}{\mathrm{d}t}\left(v_i + \frac{1}{40}d_p^2 \frac{\partial^2 \tilde{u}_i}{\partial x_j\, \partial x_j}\right)\right] \\ &+ \frac{3}{2}C_H \frac{\mathscr{V}_p}{d_p}\sqrt{\frac{\bar{\rho}_f \tilde{\mu}_f}{\pi}}\int_0^t \frac{\dfrac{\mathrm{d}}{\mathrm{d}\tau}\left(\tilde{u}_i - v_i + \dfrac{1}{24}d_p^2 \dfrac{\partial^2 \tilde{u}_i}{\partial x_j\, \partial x_j}\right)}{\sqrt{t-\tau}}\mathrm{d}\tau \\ &+ 16.3 C_S \sqrt{\bar{\rho}_f \tilde{\mu}_f}\frac{\mathscr{V}_p}{\pi d_p}\frac{\tilde{S}_{ij}}{(\tilde{S}_{lk}\tilde{S}_{lk})^{1/4}}(\tilde{u}_j - v_j) - \frac{3}{5}\pi \mu d_p \frac{2k_f^2}{\tilde{p}(2k_f + k_p)}\frac{\partial \tilde{T}_f}{\partial x_i}\end{aligned} \tag{2}$$

where $\tilde{u}_i$ and v_i represent the local filtered gas-phase velocity and the particle velocity, respectively. The variables ρ_p, $\mathscr{V}_p$, d_p, and k_p represent the particle density, volume, diameter and thermal conductivity, respectively, and $\bar{\rho}_f$, $\tilde{\mu}_f$, $\tilde{T}_f$, $\tilde{p}$, and k_f represent the gas filtered density, molecular viscosity, temperature, pressure, and thermal conductivity, respectively.

The time derivatives of the fluid velocity in the above equation are defined as the fluid acceleration:

$$\frac{D\tilde{u}_i}{Dt} = \frac{\partial \tilde{u}_i}{\partial t} + \tilde{u}_j \frac{\partial \tilde{u}_i}{\partial x_j} \tag{3}$$

and the time derivative of the fluid velocity along the particle path:

$$\frac{\mathrm{d}\tilde{u}_i}{\mathrm{d}t} = \frac{\partial \tilde{u}_i}{\partial t} + v_j \frac{\partial \tilde{u}_i}{\partial x_j} \tag{4}$$

The resolved fluid strain rate tensor is defined by:

$$\tilde{S}_{ij} = \frac{1}{2}\left(\frac{\partial \tilde{u}_i}{\partial x_j} + \frac{\partial \tilde{u}_j}{\partial x_i}\right) \tag{5}$$

The first four terms on the right-hand-side of (2) represent the conventional BBO equation. The first of these terms is the aerodynamic drag force, where the coefficient of drag is expressed as (Clift et al., 1978):

$$C_D = \begin{cases} \dfrac{24}{Re_p}\left[1 + \dfrac{3}{16}Re_p\right] & \text{for } Re_p \le 0.01 \\ \dfrac{24}{Re_p}\left[1 + 0.1315\ Re_p^{(0.82-0.05w)}\right] & \text{for } 0.01 < Re_p \le 20 \end{cases} \tag{6}$$

where $w = \log_{10} Re_p$ and the particle Reynolds number is:

$$Re_p = \frac{\bar{\rho}_f \mid \tilde{u}_i - v_i \mid d_p}{\tilde{\mu}_f} \tag{7}$$

The second of these terms represents the pressure gradient force, which would normally act to accelerate the fluid if the discrete particle were not present. The third term represents the added mass force, which accounts for the virtual mass effects of fluid entrainment around an accelerating particle. The parameter C_A is an experimentally-determined correlation which corrects for the effects of finite particle Reynolds number, and can be expressed as (Odar and Hamilton, 1964):

$$C_A = 1.05 - \frac{0.066}{Ac^2 + 0.12} \tag{8}$$

in terms of the nondimensional particle acceleration number:

$$Ac = \frac{\mid \tilde{u}_i - v_i \mid^2}{d_p \left| \frac{\mathrm{d}\tilde{u}_j}{\mathrm{d}t} - \frac{\mathrm{d}v_j}{\mathrm{d}t} \right|} \tag{9}$$

The fourth term is the Basset time history force, which accounts for the effects of residual vorticity and velocity gradients in the carrier fluid generated by a nonuniformly-accelerating particle. Again, a correction for finite particle Reynolds number is included, expressed as (Odar and Hamilton, 1964):

$$C_H = 2.88 + \frac{3.12}{(Ac + 1)^3} \tag{10}$$

The fifth term in the particle momentum equation accounts for the inertial lift force felt by a particle with a relative velocity in a shear flow. The form shown is a two-dimensional generalization of the one-dimensional result derived by Saffman (1965, 1968). The constraints on this equation of low particle Reynolds numbers and low fluid shear rates are relaxed by the term (Mei, 1992):

$$C_S = \begin{cases} (1 - 0.3314\alpha^{1/2}) \exp\left(- \frac{Re_p}{10} \right) + 0.3314\alpha^{1/2} & \text{for } Re_p \leq 40 \\ 0.0524(\alpha\ Re_p)^{1/2} & \text{for } Re_p > 40 \end{cases} \tag{11}$$

where:

$$\alpha = \frac{\mid \tilde{S}_{ij} \mid d_p}{\sqrt{2} \mid \tilde{u}_i - v_i \mid} \tag{12}$$

Note that the constant in Saffman's original expression has been modified by a factor of $2^{3/4}$ and the fluid shear rate has been modified by a factor of $2^{1/2}$ so that these expressions in terms of the fluid strain rate tensor reduce identically to Saffman's original expression for one-dimensional shear flow.

The final term in the particle momentum equation models the force due to thermophoresis, which results when gas molecules surrounding a body exert an unevenly-distributed thermal pressure, which occurs when a temperature gradient exists in the gas. The equation shown takes the form of a simplified model presented by Davies (1966).

The second-order spatial derivatives in the aerodynamic drag, added mass, and Basset history expressions are the Faxen correction terms (Maxey and Riley, 1983). These supply a first-order approximation to the effects of streamline curvature in the vicinity of the sphere, and can be neglected for spheres that are small with respect to the dominant shear length scales in the flow. This assumption will be made here since typical spray droplets or suspended particles are quite small with respect to the Kolmogorov length scale of turbulence in practical combustion environments (Shirolkar et al., 1996).

Each discrete particle trajectory is determined by integrating the particle momentum equation in conjunction with:

$$\frac{\mathrm{d}x_{p,i}}{\mathrm{d}t} = v_i \tag{13}$$

where $x_{p,i}$ is the particle position. The temperature is specified by solving the energy equation for a spherical, nonevaporating particle with convection heat transfer. Since the Biot number is less than 0.1 for all cases studied here, the particles can be assumed to have a uniform internal temperature (Incropera and DeWitt, 1996). The energy equation then reduces to:

$$\rho_p \mathcal{V}_p C \frac{\mathrm{d}T_p}{\mathrm{d}t} = \pi d_p k_f \, Nu(\tilde{T}_f - T_p) \tag{14}$$

where C is the particle specific heat and Nu is the particle Nusselt number approximated by the Ranz–Marshall correlation as (Zhou, 1993):

$$Nu = 2 + 0.6 \, Pr^{1/3} \, Re_p^{1/2} \tag{15}$$

These ordinary differential equations governing particle motion and heat transfer are integrated using the second-order Runge–Kutta technique, which provides excellent accuracy with the small time steps required by the LES numerical method. The Eulerian flow variables are interpolated to each discrete particle position using third-order Lagrange polynomials.

2.3. Governing nondimensional parameters

A detailed order-of-magnitude analysis can show that for $\rho_p/\rho_f \approx 10^3$, as studied here, the aerodynamic drag force typically dominates all other forces in (2) (Lazaro and Lasheras, 1989). Under this assumption, the particle momentum equation reduces to:

$$\frac{\mathrm{d}v_i}{\mathrm{d}t} = \frac{(\tilde{u}_i - v_i)}{\tau_v} f(Re_p) \tag{16}$$

where the velocity relaxation time is defined as:

$$\tau_v = \frac{\rho_p d_p^2}{18\tilde{\mu}_f} \tag{17}$$

and $f(Re_p)$ is a correction to Stokes drag for finite Reynolds numbers, represented by the bracketed terms in (6). The value of $f(Re_p)$ will always tend toward unity, so the time scale τ_v closely correlates the particle responsiveness to changes in the fluid velocity. From this, the Stokes number is then defined as:

$$St = \frac{\tau_v}{\tau_f} \tag{18}$$

where τ_f is a dominant time scale of the fluid motion. Following Aggarwal et al. (1994), the best correlation of particle motion in jet shear flows can be obtained with τ_f defined in terms of the jet preferred-mode frequency as $\tau_f = 1/f_p$. With this definition, the particle dispersion with respect to the large-scale, coherent vortical structures of the shear layer can be characterized.

The particle energy equation (14) can be similarly reduced to the form:

$$\frac{\mathrm{d}T_p}{\mathrm{d}t} = \frac{(\tilde{T}_f - T_p)}{\tau_T}\left(\frac{Nu(Re_p, Pr)}{2}\right) \tag{19}$$

where the temperature relaxation time is:

$$\tau_T = \frac{\rho_p C d_p^2}{12 k_f} \tag{20}$$

which characterizes the particle responsiveness to changes in the surrounding thermal environment.

This time scale can be rewritten in the form:

$$\tau_T = \tfrac{3}{2}\beta\ Pr\ \tau_v \tag{21}$$

where $\beta = C/c_\mathrm{p}$, c_p is the gas constant-pressure specific heat, and τ_v is the previously defined velocity relaxation time. Thus, the particle properties that govern spatial dispersion also contribute to the thermal response, so that the spatial and thermal particle behavior are inherently coupled. In this study, a constant value of τ_f is used to define the Stokes number in (18). Therefore, for convenience, the particle thermal behavior is assumed to be a primary function of St and the parameter group $\beta\ Pr$, where an increase in either parameter is expected to result in a particle that responds more slowly to changes in the surrounding thermal environment.

In (2) the LES filtered gas velocity is used to model the particle behavior. Neglecting the velocity fluctuations of the unresolved eddies will generally introduce an error to the solution, and so the validity of this approximation should be estimated. The largest unresolved eddies will most likely introduce the largest error. On the present computational grid, it is found that particles with a Stokes number of 0.01 have roughly the same velocity relaxation time as the time scale of these largest unresolved eddies. The particles of interest in this study have a

Stokes number roughly two orders-of-magnitude larger than this value, so it is assumed here that neglecting the unresolved subgrid-scale eddies is acceptable to model the particle behavior. Similar assumptions have been made in other studies, where LES and DNS results were compared to demonstrate that a majority of particle sizes are indeed unaffected by unresolved fluctuations (e.g. Wang and Squires, 1996a; Uijttewaal and Oliemans, 1996).

2.4. Statistical measures

Nearly all numerical studies to date in the literature on particle behavior in shear flows quantify the spatial dispersion as an RMS change in transverse particle position as it differs from either the initial position or a mean transverse position, summed over all particles in the domain at a particular instant in time. This will be referred to as total dispersion, and will be calculated here as:

$$(D_y^p)_{\text{tot}}(t) = \left[\frac{1}{N_{\text{tot}}} \sum_{i=1}^{N_{\text{tot}}} (y_p^i(t) - y_p^i(t_0))^2 \right]^{1/2} \tag{22}$$

where N_{tot} is the total number of particles in the domain at time t, $y_p^i(t)$ is the transverse position of particle i at the measurement time, and $y_p^i(t_0)$ is the initial location of particle i. This statistical parameter may not give the best representation of the particle behavior, since the dispersion of particles far downstream of the injection location are averaged with particles that have just been injected, which have not yet interacted significantly with the shear layer vortices. Therefore, this parameter will be used only to perform limited comparisons with existing results in the literature, found in Section 3.2.

All other spatial dispersion results presented in this paper will be calculated as:

$$D_y^p(x) = \left[\frac{1}{N} \sum_{i=1}^{N} (y_p^i(x) - y_p^i(x_0))^2 \right]^{1/2} \tag{23}$$

where N is the number of particles that have passed axial position x throughout the entire simulation, $y_p^i(x)$ is the transverse position of particle i as it passes this measurement point, and $y_p^i(x_0)$ is the initial transverse position of the particle. This form of the spatial dispersion represents an axially-developing measure of the transverse particle position as it differs from the injection value. This way, a clear picture of the particle dispersion behavior can be obtained at specific locations downstream of the jet nozzle.

Additionally, the heating characteristics of particles will be quantified by thermal dispersion statistics, which are calculated identically to spatial dispersion as:

$$D_T^p(x) = \left[\frac{1}{N} \sum_{i=1}^{N} (T_p^i(x) - T_p^i(x_0))^2 \right]^{1/2} \tag{24}$$

where $T_p^i(x)$ and $T_p^i(x_0)$ are the particle temperatures at the measurement position and the initial location, respectively. In the present study, this parameter should be viewed only as a

measure of the mean particle temperature increase, since each particle is injected at the temperature of the cool unreacted gas.

It is assumed in this study that the particles in each injection stream are widely-spaced enough that they do not interact with each other or alter the gas-phase properties significantly. The statistical measures presented above are nearly independent of particle spacing in each injection stream, although they tend to converge faster for a more rapid particle injection. To speed convergence, the one-way coupled assumption is maintained while the particle injection rate is increased to an optimum value. Here, this is an injection at every fourth time step. Also, since the calculations are one-way coupled, many separate particle studies may be performed simultaneously in a single gas-phase simulation without altering any of the gas properties. This eliminates redundant LES runs without sacrificing any accuracy of the results.

An initial test simulation was run until all statistical parameters converged to a constant value. A total simulation length was then selected to ensure that all statistics converged to well-within 5% of their final value. This simulation time was selected to be 500 nondimensional time units, defined as $t^* = t\Delta U/D$. The sensitivity of results to fluid property interpolation order was also investigated. First-, second-, and third-order Lagrange polynomial interpolation was tested, with minimal differences in the calculated statistical results (Glaze, 1998). Third-order interpolation was finally selected to eliminate any doubt about the accuracy.

3. Results

3.1. Importance of unsteady terms in particle momentum equation

The quasi-steady aerodynamic drag term in the particle momentum equation typically dominates the remaining terms, which will henceforth be called the unsteady forces. Recent studies have shown the importance of these forces in several fundamental flows, such as homogeneous turbulence, boundary layers, and acoustically-oscillating flow (e.g. Dodemand et al., 1995; Wang et al., 1997; Vojir and Michaelides, 1994). However, the importance of these forces in nonhomogeneous reacting shear flows is not known. Although the unsteady forces can be proven small by dimensional arguments, even a small change in the initial trajectory can significantly affect the particle temperature characteristics far downstream, where large temperature gradients exist in the vicinity of the flame. Thus, the importance of the unsteady terms should be investigated before continuing because neglecting them would greatly simplify the analysis.

The thermophoresis force in (2) is typically less than 0.2% of the dominant aerodynamic drag force for the smallest particles studied here, and is even less for larger particles. Therefore, it will not be considered. For faster reaction rates or higher heat release rates than studied here, the larger temperature gradients may require the inclusion of this force. In general, thermophoresis should not be neglected in realistic reacting flows.

For brevity, a complete study of the effects of the unsteady forces will not be presented here, but can be found in Glaze (1998). Typical particle behavior will be shown under the influence of these forces to illustrate their relative importance in a flow configuration such as this. Fig. 2 illustrates the trajectories of six particles with a Stokes number of 0.5, injected at locations

from the centerline through the center of the shear layer. The two curves from each initial location represent the particle trajectory if it is acted on by either the aerodynamic drag force or a summation of all forces, where both cases are calculated simultaneously in a single jet simulation. The six particles were injected at three different initial velocities, consisting of a velocity half of the local gas velocity, a velocity equal to the gas velocity, and a velocity twice the gas velocity. For the equilibrium injection velocity, neglecting the unsteady forces makes little difference in the particle behavior. If the particles have an initial velocity excess or deficit when compared to the local gas velocity, the unsteady forces may alter the trajectory significantly. It should be mentioned that the specific time of injection with respect to the vortex shedding of the shear layer will alter the particle behavior from that shown here, although these results are typical. The trajectories of particles with either large or small Stokes numbers are not significantly affected by the unsteady forces in this type of flow, and are not illustrated here.

The different particle behavior under the influence of the unsteady forces can be attributed primarily to the Basset time history force and the Saffman lift force, both having typical magnitudes on the order of 10% of aerodynamic drag for the nonequilibrium initial velocities shown in Fig. 2. The remaining forces are generally an order of magnitude less than the Basset and Saffman forces for this flow geometry, and contribute little to the particle behavior.

The effect of the differing trajectories on the temperature of these particles is shown in Fig. 3 for the two particles injected closest to the shear layer. Again, the particle injected at a velocity equilibrium behaves nearly the same both with and without the unsteady forces. The particles injected faster or slower than the gas velocity can have much different temperature histories due to their interactions with different regions surrounding the flame. Thus, for nonequilibrium

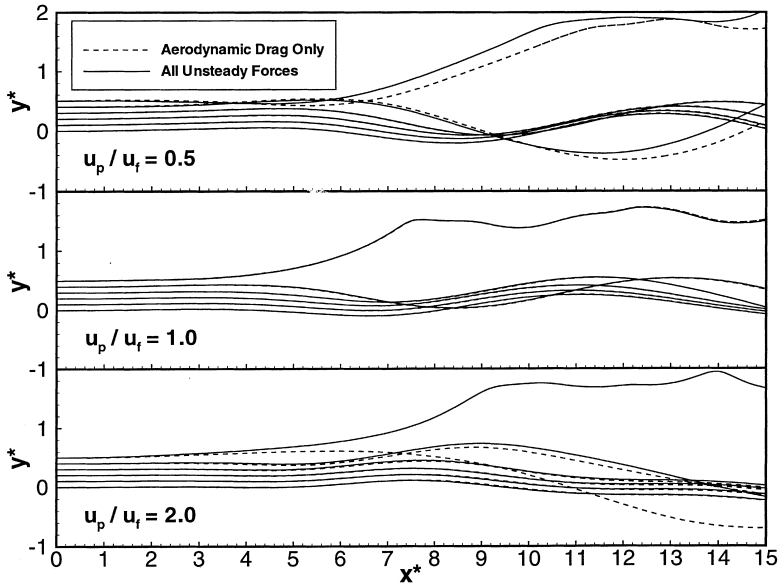

Fig. 2. Particle trajectories both with and without inclusion of the unsteady forces for particles injected into the shear layer at a velocity half, equal to, and twice the local gas velocity.

initial velocities, detailed simulations of particle heat-up, evaporation, or combustion may require the inclusion of these forces for acceptable accuracy.

For the most general results, mean particle behavior for an equilibrium initial velocity will be considered here. Hence, all unsteady forces can be safely neglected, so that the particles are guided by aerodynamic drag only.

3.2. Spatial dispersion results

Quantitative comparisons between the present simulations and existing experimental and numerical results in the literature is challenging because of the low jet Reynolds number studied here as well as the two-dimensional structure of the co-flowing jet. However, limited comparisons are possible by studying particle spatial dispersion which has been normalized by the dispersion of fluid tracer particles. This statistical parameter goes some of the way toward eliminating the effects of flow geometry and the Reynolds number, while still capturing the dominant particle behavior as a function of the Stokes number. To be consistent with existing computational studies, this parameter is defined as:

$$\gamma_D = \frac{(D_y^p)_{\mathrm{tot}}(t)}{(D_y^f)_{\mathrm{tot}}(t)} \tag{25}$$

where the total particle spatial dispersion $(D_y^p)_{\mathrm{tot}}(t)$ is defined in (22). The new fluid tracer particle dispersion $(D_y^f)_{\mathrm{tot}}$ is defined identically to $(D_y^p)_{\mathrm{tot}}(t)$, except that it is calculated for fluid tracer particles with the same initial conditions.

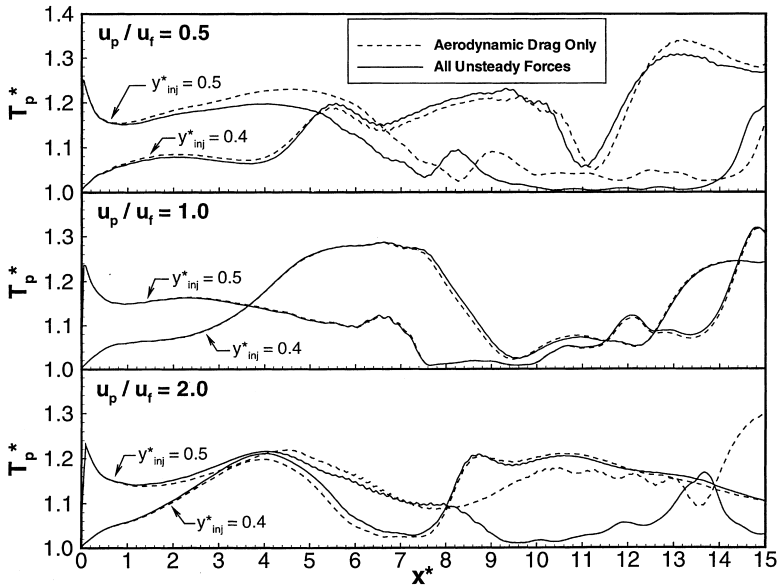

Fig. 3. Particle temperatures both with and without inclusion of the unsteady forces for particles injected into the shear layer at a velocity half, equal to, and twice the local gas velocity.

Comparisons of this normalized dispersion in a nonreacting jet with data from the studies of Chung and Troutt (1988) and Uthuppan et al. (1994) are shown in Fig. 4. Note that both of these studies were performed at a Reynolds number of 200,000 and they simulate an axisymmetric jet issuing into a quiescent environment. The present planar-jet simulation is performed at a Reynolds number of 1000, and there is a co-flowing oxidizer stream surrounding the core fuel jet. The definition of the Stokes number in these two studies also differs from the present study. The fluid time scale τ_f in Eq. (18) may be defined somewhat arbitrarily, as long as it is a good measure of a dominant time scale in the fluid motion (Aggarwal et al., 1994). Chung and Troutt chose to define it as $\tau_f = D/U_0$, where D is their jet diameter and U_0 is their jet velocity. The instability frequency of their jet is such that this time scale is almost identical to the time scale of their vortex shedding, so that this definition is entirely equivalent to that used in the present study. Uthuppan et al. chose to define their fluid time scale as $\tau_f = 4/f$, where f is the vortex shedding frequency. This parameter is meant to represent the time scale of the second vortex pairing. This is also roughly equivalent to the definition used in the present study because of the tendency of their vortex rings to undergo strong, early pairing events very close to the jet nozzle before significant particle interactions have occurred. In addition, these studies chose to measure the normalized spatial dispersion at different times, although both studies selected the time at which the dispersion approaches a constant value. To be consistent, the same selection was made here. This nondimensional measurement time was chose to be 12, where the nondimensional time is defined at $t^* = t\Delta U/D$.

The differences between the curves in Fig. 4 are most likely attributed to the different simplifying assumptions, numerical methods, and flow geometries used in each study. Despite these differences, the results in Fig. 4 show a remarkable level of similarity with the data of Aggarwal et al. The data of Chung and Troutt does not follows as closely the other two data sets in this figure, although the overall trends are similar. All of these studies indicate that particles with a Stokes number near unity are preferentially-dispersed over both larger and

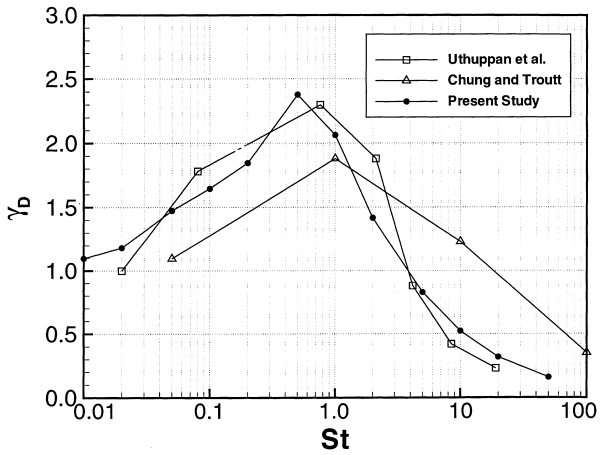

Fig. 4. Comparison of normalized total spatial dispersion in a nonreacting jet with results from previous numerical studies.

smaller particles. This is a consistent trend seen in nearly all computational and experimental studies (Aggarwal et al., 1994).

The trend of particles gathering in regions of low vorticity and high strain rate is also a common observation in recent experimental particle transport studies of both nonreacting (Longmire and Eaton, 1992; Swanson and Richards, 1997; Ye and Richards, 1996; Ye et al., 1995) and reacting jets (Eickmann and Richards, 1997). This same behavior is observed here in Fig. 5, which shows the dispersion patterns for three different particle sizes superimposed on a plot of vorticity magnitude in a nonreacting jet. It is clear from these illustrations that the

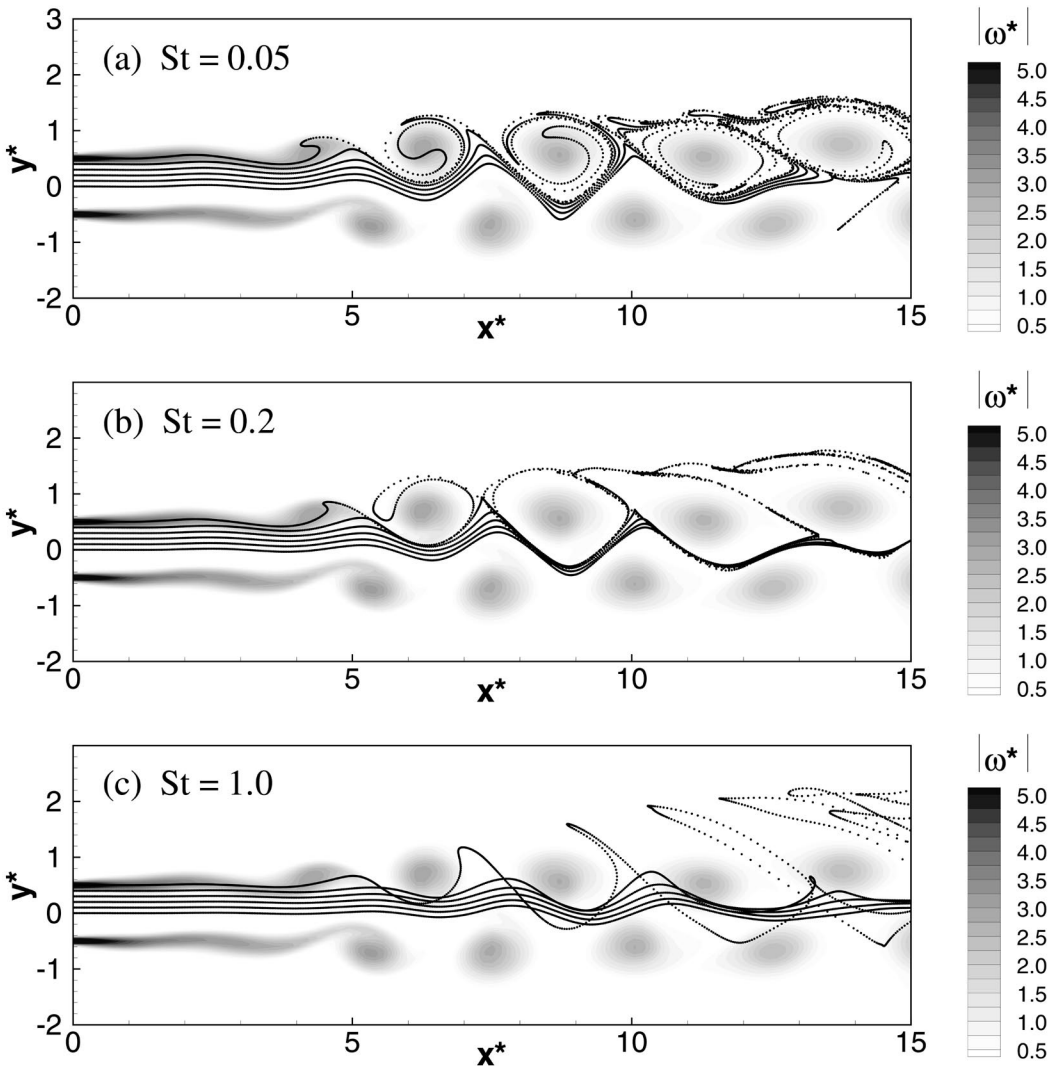

Fig. 5. Effect of vorticity on particle dispersion patterns in a nonreacting jet.

centrifugal force generated by the shear layer vortices is the prime cause of particle dispersion for a wide range of particle sizes.

Eq. (23) will now be used to calculate the axial development of spatial dispersion for particles injected directly into the shear layer, shown in Fig. 6. Far upstream in the jet, before any coherent vortical structures have formed in the shear layer, it is the smallest particles that disperse the most due to their small inertia which allows them to closely follow the fluid motion. Far downstream after interacting with these vortical structures, intermediate-sized particles disperse more than both larger or smaller particles, with a Stokes number of unity being optimally-dispersed near the exit of the computational domain. These trends measured far downstream are the same as those previously seen in Fig. 4. This is also consistent with a majority of published experimental and computational results.

The spatial dispersion behavior also depends strongly on the initial location within the jet nozzle, which can be qualitatively seen in Fig. 5. These particle/vortex interactions are quantified in terms of the spatial dispersion statistics shown in Fig. 7, for a nonreacting jet. Here, the particle dispersion is plotted as a function of the Stokes number for six injection locations between the centerline of the jet ($y^*_{\mathrm{inj}}=0.0$) and the shear layer ($y^*_{\mathrm{inj}}=0.5$). Figs. 7(a)–(c) represent results gathered at 4, 8, and 12 jet widths downstream of injection, respectively. In Fig. 7(a), upstream of any significant interactions with the shear layer structures, it is consistently the smaller particles that spatially disperse the most for all injection locations. Looking farther downstream, Fig. 7(b) shows that for injection locations near the shear layer, particles with an intermediate size are scattered more than both smaller and larger particles. Here, the smaller particles closely follow the vortical fluid motion while the larger particles follow a nearly linear path guided primarily by their own inertia. The intermediate-sized particles can be radially accelerated from the core of the shear layer vortices by centrifugal force, with their sizeable inertia allowing them to maintain this velocity long enough to be scattered farther than both smaller and larger particles. From this figure, it can be seen that as the initial location is moved closer to the shear layer, the preferentially-dispersed Stokes number shifts towards larger particle sizes. These injection locations allow the particles to interact closer to the cores of the shear layer vortices, where the larger particles are able to undergo a stronger acceleration in this faster-rotating fluid. Even farther downstream,

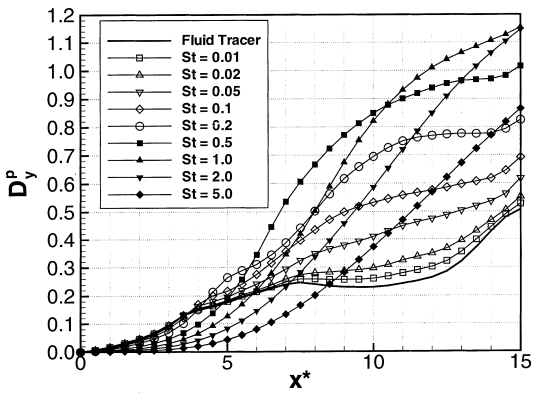

Fig. 6. Spatial dispersion development along the axis of a nonreacting jet for particles injected into the shear layer.

Fig. 7(c) shows that the overall dispersion trends are similar. However, the preferentially-dispersed range of particle sizes has consistently shifted toward larger particles, simply because these larger particles require more interaction time to be accelerated and scattered.

While the results presented thus far have been for particles in a nonreacting jet, Fig. 8 shows a comparison of this behavior with that in a reacting jet for fluid tracer particles. The probability density functions of transverse particle position shown here has a consistently larger standard deviation for the nonreacting case. This enhanced particle scattering in the nonreacting jet can be explained primarily by the temperature-dependent viscosity difference between the two jets. In the reacting jet, the viscosity will be higher in the vicinity of the flame. This overall higher viscosity leads to a lower turbulent mixing rate in the reacting jet, hindering the particle dispersion. Fig. 9 shows the behavior of particles with inertia of their own, with a Stokes number of 0.5. Here, the particle behavior for the two cases is much more similar, although a slight dispersion enhancement can still be seen in the nonreacting jet. For even larger particles than this, differences become negligible. From these results, the spatial

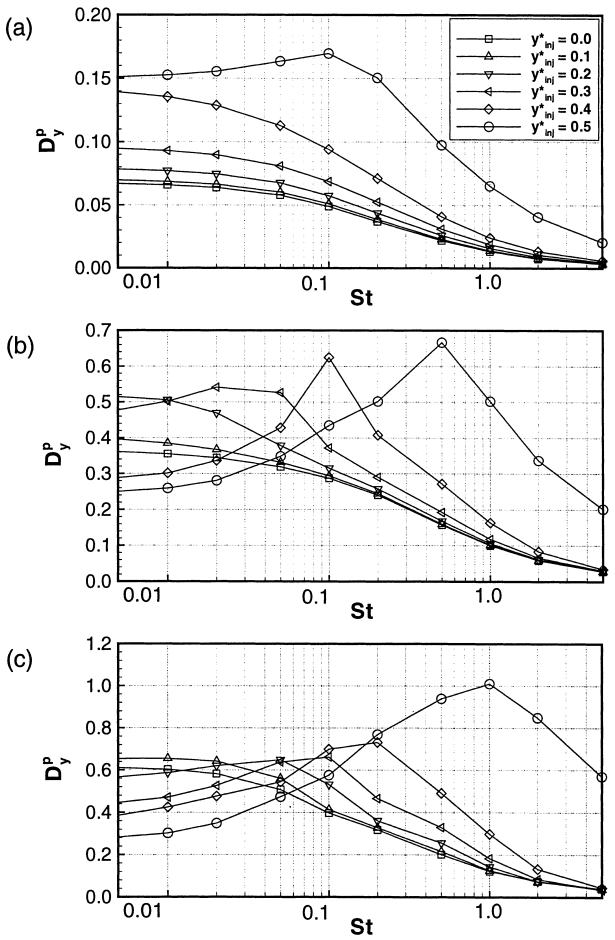

Fig. 7. Spatial dispersion at axial locations of (a) $x^*=4$, (b) $x^*=8$, and (c) $x^*=12$.

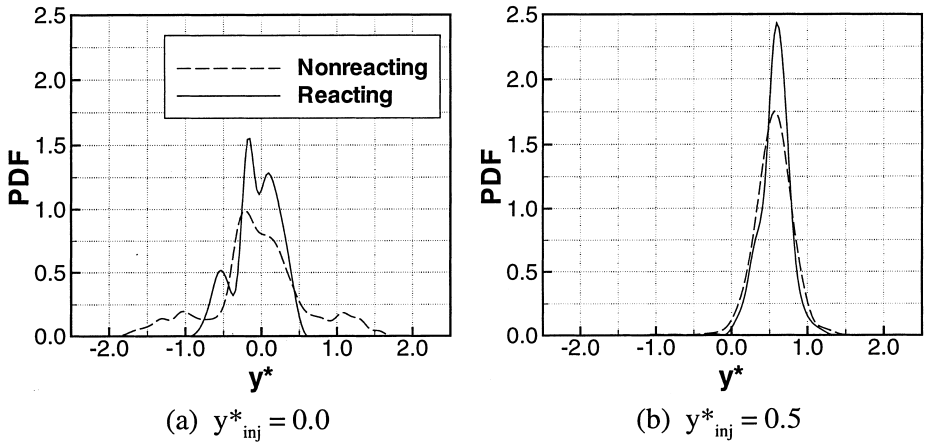

Fig. 8. Comparison of transverse particle position PDFs for fluid tracer particles in both a reacting and a nonreacting jet, measured at $x^* = 12$.

dispersion trends are almost identical in a reacting and a nonreacting jet, with the largest difference being only for the smallest particles. If a faster chemical reaction or a higher heat release rate is simulated, the differences between a reacting jet and nonreacting jet will almost certainly be enhanced over what is demonstrated here.

3.3. Thermal results

Fig. 10 shows the thermal dispersion, calculated with (24), of particles with several sizes and material properties. These results are measured at an axial location of eight jet slot widths downstream of injection. Here, the results are plotted as a function of the Stokes number for

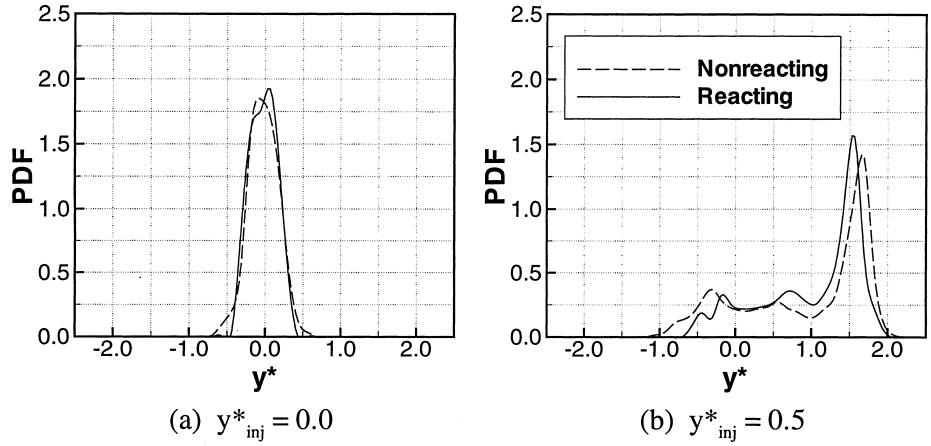

Fig. 9. Comparison of transverse particle position PDFs for particles with $St = 0.5$ in both a reacting and a nonreacting jet, measured at $x^* = 12$.

curves of constant values of the previously-discussed thermal parameter, $\beta\ Pr$. In practical applications, $\beta\ Pr$ can cover a wide range of values depending on the specific combination of particle materials and gas composition. For example, metal particles in air tend to have low $\beta\ Pr$ values between 0.05 and 1.0, while water droplets in air have a relatively high value of approximately 3.0. Fuel sprays of hydrocarbon or alcohol droplets in a gaseous mixture of air and the vaporized fuel may have values between 0.5 and 5.0. It should be noted that the extremely large or small values at either end of the $\beta\ Pr$ range studied here cannot be reached by practical substances, and are included only for the purpose of demonstrating the asymptotic behavior of the limiting cases.

From the definition of the thermal relaxation time in (21), it is expected that an increase in either $\beta\ Pr$ or St would lead to a particle that heats less rapidly. For nearly all injection locations and Stokes numbers, Fig. 10 shows that as $\beta\ Pr$ is increased, the particles heat less

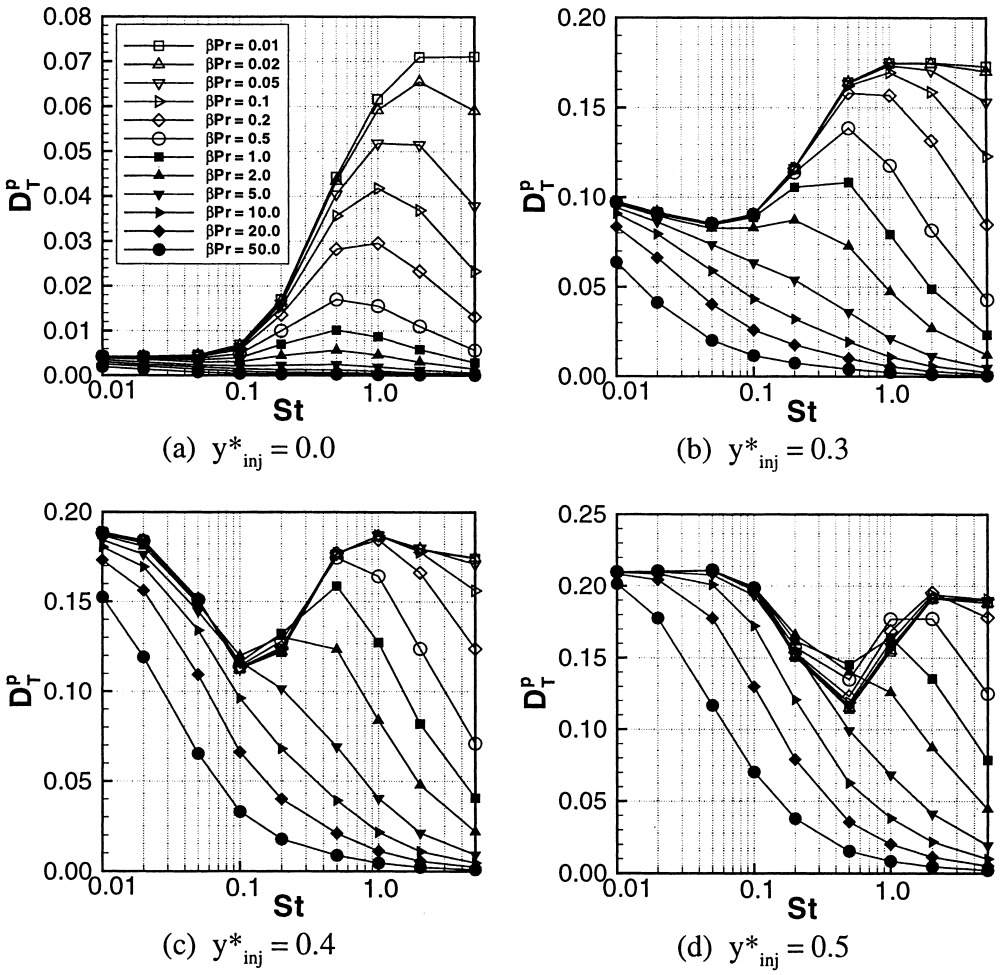

Fig. 10. Thermal dispersion for four discrete particle injection locations, measured at $x^* = 8$.

rapidly and tend toward a lower mean temperature. However, as the Stokes number is increased, a consistent heating trend is not seen. The uppermost curves in these figures correspond to the lowest value of $\beta\ Pr$, representing particles that closely approximate the gas temperature. In Fig. 10(a), these curves reveal that as the Stokes number is increased for particles injected on the jet centerline, these particles are exposed to an increasing mean gas temperature. From this, the general observation can be made that for this initial location, the larger particles are able to heat more rapidly, while the smallest particles remain near the initial temperature.

A unique trend can be seen by inspection of the curves for low $\beta\ Pr$ as the injection location is moved closer to the shear layer, shown in Figs. 10(b)–(d). As the injection location is moved closer to the shear layer, larger particles are exposed to a lower mean temperature, indicated by the trough in the uppermost curves. Interestingly, this low-temperature range exactly corresponds to the preferentially-scattered particle sizes previously seen in Fig. 7(b) at this location. Thus, a high spatial dispersion, which is sometimes associated with good particle mixing, does not necessarily lead to particles that heat rapidly in this jet flame.

This counterintuitive result can be explained by observing some detailed flow visualizations

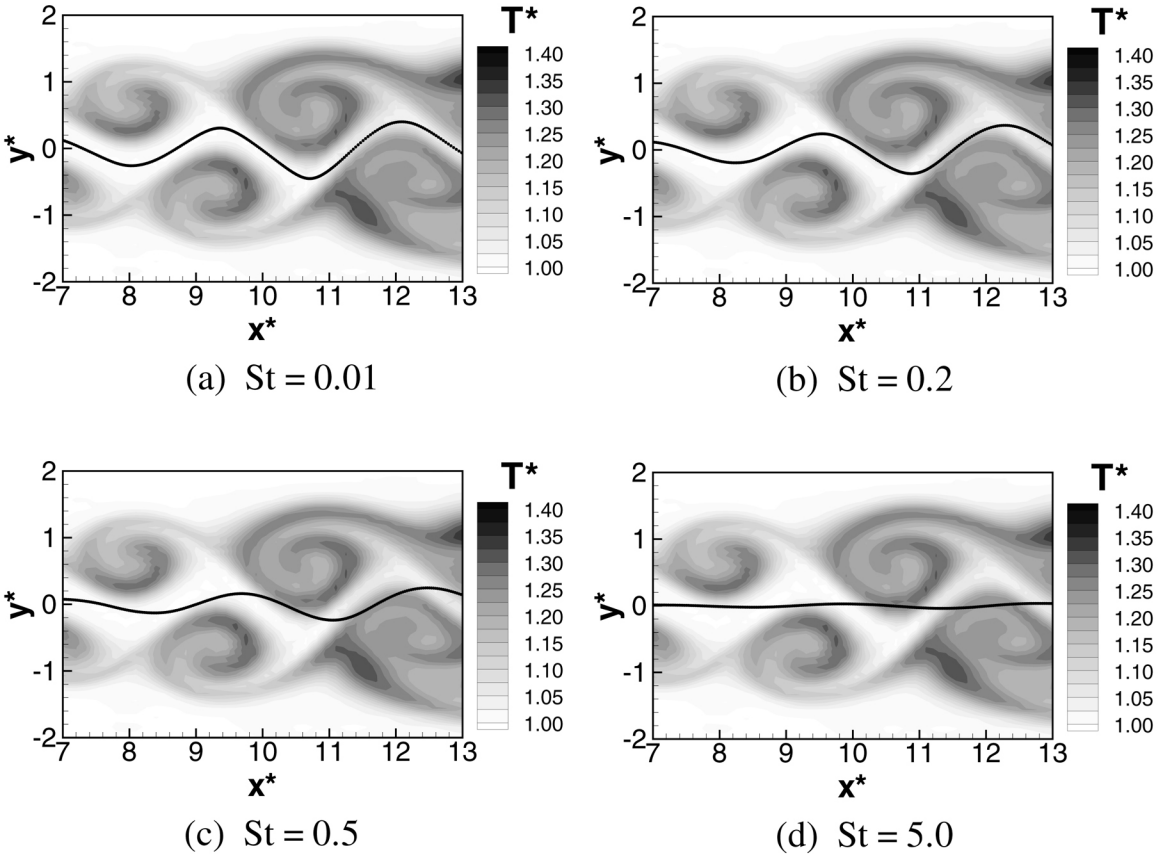

Fig. 11. Particle/vortex interactions for particles injected on jet centerline.

of particle dispersion patterns in the reacting jet. Fig. 11 shows continuous streams of four different particle sizes injected on the jet centerline, superimposed on a plot of gas temperature at a location far downstream from injection. Fig. 11(a) illustrates how small particles, of $St = 0.01$, closely follow the oscillatory motion of the jet centerline. These particles remain in the cool unreacted fuel of the jet core, never mixing with the high-temperature regions near the flame. As the particle size is increased toward the largest size of $St = 5.0$, shown in Fig. 11(d), the particles follow an increasingly-linear path under the influence of their increased inertia. These particles are able to intermittently cut directly through the high-temperature regions surrounding the flame, leading to a higher mean temperature. This explains the unusual temperature increase seen for larger particles in Fig. 10(a), which have a larger thermal capacity and would have been expected to heat more slowly.

Fig. 12 illustrates results for the same four particle sizes injected into the center of the shear layer. Here, the smallest particles are dispersed throughout the high-temperature core of the vortices, leading to a high mean particle temperature. The largest particles are able to cut directly through the reacting regions of the vortices, also leading to a high mean particle temperature. The mid-sized particles, however, behave differently. Fig. 12(b) and (c) show two

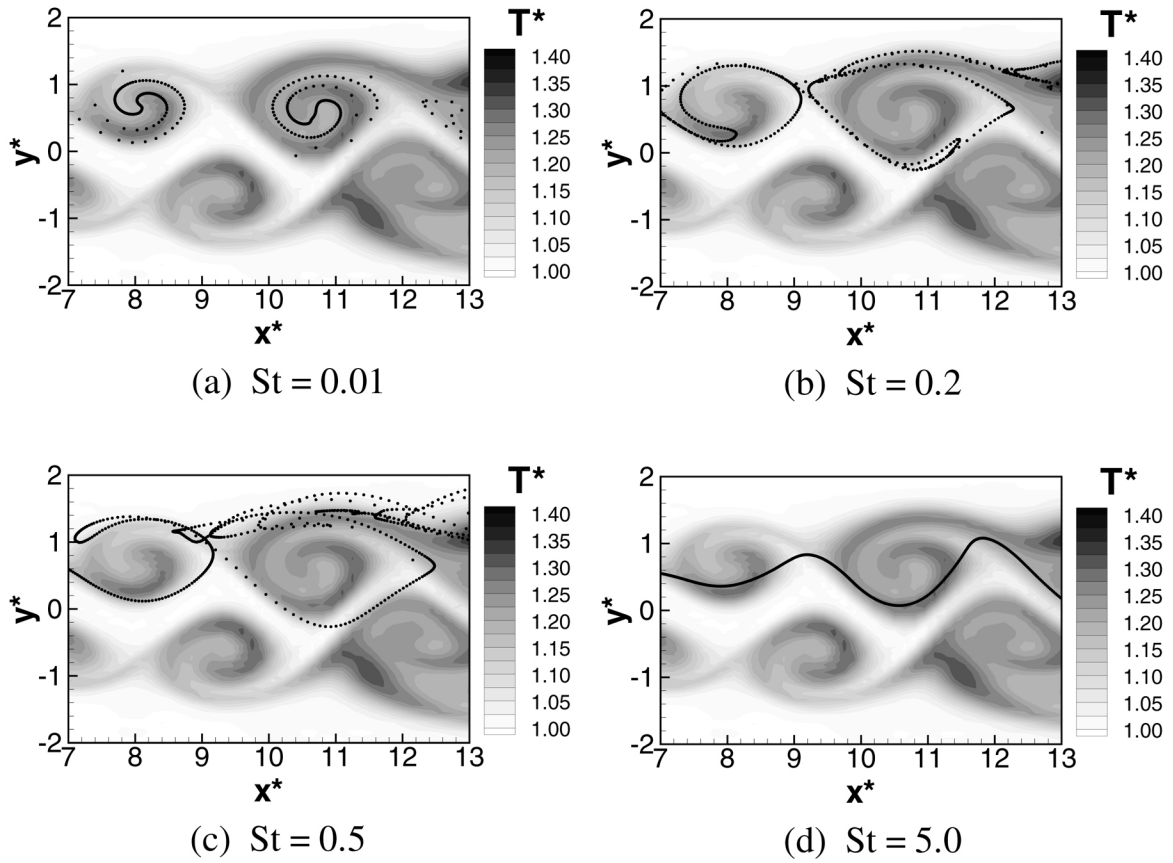

Fig. 12. Particle/vortex interactions for particles injected into the shear layer.

intermediate-sized particles, which were previously seen to have a large spatial dispersion for this injection location. Here, it can be seen that these particles are actually driven by centrifugal force away from the high-temperature reacting regions near the vortex cores. This explains the trends previously seen in Fig. 10(d) where an intermediate-sized particle can heat less than both small and large particles. Although not shown, the same trend of a large spatial dispersion leading to a lower particle temperature also occurs in both upstream and downstream locations. This confirms the suspected coupling between spatial dispersion and particle temperature in this type of flow geometry.

4. Summary and concluding remarks

A numerical simulation of the spatial dispersion and heating trends of inert particles in a nonpremixed jet flame have been performed. From these results, it is clear that there is a strong coupling between the spatial and thermal particle behavior in this type of a nonhomogeneous thermal environment. Consistent with earlier published results, it has been shown that particles with a small Stokes number closely follow the fluid motion, while particles with a large Stokes number follow a trajectory guided by their own inertia. Particles with a Stokes number near unity can be significantly scattered from the shear layer vortices due to centrifugal force.

The thermal behavior of inert particles has been characterized in terms of their Stokes number and the thermal parameter group $\beta\ Pr$. It has been shown that as $\beta\ Pr$ is increased, the particles heat more slowly and have a lower mean temperature at downstream locations. The Stokes number affects the thermal capacity of particles, as well as their spatial dispersion behavior. In fact, it is the intermediate-sized, highly-scattered particles with a Stokes number near unity that can be thrown from the high-temperature, reacting regions of the jet into cooler nonreacting flow. For a majority of initial locations, both smaller and larger particles are generally able to interact directly with the flame in the jet, leading to a higher mean temperature.

It has also been briefly shown that the unsteady terms in the particle momentum equation may be important in this type of flow geometry. When the particles are injected into the jet with a velocity either faster or slower than the local gas velocity, the unsteady forces may alter the particle trajectories enough to place them in a significantly different thermal environment. Neglecting these forces may distort results that depend on the precise thermal history, such as evaporation or combustion. Thus, their importance should be investigated in realistic reacting shear flow simulations.

It should be emphasized that the results presented in this study were based on idealized simulations that have been simplified to make the problem computationally tractable. For a higher reaction rate or heat release rate, the flame/vortex interactions may be significantly different. If the flame location or behavior is changed, then the particle heating trends would most certainly be different from those presented in this study. Realistic reacting two-phase flows, such as spray flames and pulverized coal combustors, also involve the strong two-way coupling effects of droplet or particle evaporation and reaction, as well as more complicated flow geometries than the two-dimensional co-flow jet studied here. Thus, these results should

not be viewed as being directly applicable to all flows. Large-scale, coherent vortical structures are, however, a fundamental turbulent structure that can be found in most reacting shear flows. The results presented in this study can therefore be viewed as an introduction to the types of particle/vortex interactions that can occur in this type of nonisothermal structure. It can be observed from these results that advanced simulations of droplet evaporation and reaction will almost certainly require a time-accurate numerical formulation as used in this study. Simple, time-averaged approaches may not be able to capture the detailed particle/vortex interactions demonstrated here.

Acknowledgements

Partial funding for this research was provided by the U.S. Office of Naval Research (ONR) under ONR contract number N00014-95-1-0623 with Dr. Gabriel Roy serving as technical monitor.

References

Aggarwal, S.K., Park, T.W., Katta, V.R., 1996a. Unsteady spray behavior in a heated jet shear layer: droplet–vortex interactions. Combust. Sci. Tech. 113–114, 429–449.

Aggarwal, S.K., Xiao, Y., Uthuppan, J., 1994. Effect of Stokes number on particle dispersion. Atomization and Sprays 4, 223–236.

Aggarwal, K., Yapo, J.B., Grinstein, F.F., Kailasanath, K., 1996b. Numerical simulation of particle transport in planar shear layers. Comput. and Fluids 25, 39–59.

Brown, G.L., Roshko, A., 1974. On density effects and large structure in turbulent mixing layers. J. Fluid Mech. 64, 775–816.

Chen, X.Q., Pereira, J.C.F., 1996. Large-eddy simulation of particle dispersion in a plane mixing layer. In: Proceedings of the 3rd International Symposium on Engineering Turbulence Modelling and Measurements. Elsevier, Amsterdam, pp. 259–271.

Chung, J.N., Troutt, T.R., 1988. Simulation of particle dispersion in an axisymmetric jet. J. Fluid Mech. 186, 199–222.

Clift, R., Grace, J.R., Weber, M.E., 1978. Bubbles, Drops, and Particles. Academic Press, New York.

Crowe, C.T., Troutt, T.R., Chung, J.N., 1996. Numerical models for two-phase turbulent flows. Ann. Rev. Fluid Mech. 28, 11–43.

Davies, C.N., 1966. Aerosol Science. Academic Press, New York.

DesJardin, P.E. 1998. Large eddy simulation of strongly radiating nonpremixed turbulent jet flames. Ph.D. thesis, School of Mechanical Engineering, Purdue University, West Lafayette, IN.

Desjardin, P.E., Frankel, S.H., 1998. Large eddy simulation of a nonpremixed reacting jet: application and assessment of subgrid-scale combustion models. Phys. Fluids 10 (9), 2298–2314.

Dodemand, E., Prud'homme, R., Kuentzmann, P., 1995. Influence of unsteady forces acting on a particle in a suspension application to the sound propagation. Int. J. Multiphase Flow 21 (1), 27–51.

Eickmann, K., Richards, C. 1997. The structure of a reacting droplet-laden forced jet. The 10th Annual Conference on Liquid Atomization and Spray Systems. ILASS, Ontario, Canada. pp. 279–283.

Elghobashi, S., 1994. On predicting particle-laden turbulent flows. Applied Scientific Research 52, 309–329.

Faeth, G.M., 1983. Evaporation and combustion of sprays. Prog. Energy Combust. Sci. 9, 1–76.

Faeth, G.M., 1987. Mixing, transport and combustion in sprays. Prog. Energy Combust. Sci. 13, 293–345.

Germano, M., Piomelli, U., Moin, P., Cabot, W.H., 1991. A dynamic subgrid-scale eddy viscosity model. Phys. Fluids A 3 (7), 1760–1765.

Glaze, D.J. 1998. A computational study of the spatial and thermal dynamics of Particles in a reacting jet. Masters thesis, School of Mechanical Engineering, Purdue University, West Lafayette, IN.

Hussain, A.K.M.F., Zaman, K.B.M.Q., 1981. The 'preferred mode' of the axisymmetric jet. J. Fluid Mech. 110, 39–71.

Incropera, F.P., DeWitt, D.P., 1996. Fundamentals of Heat and Mass Transfer. John Wiley and Sons, New York.

Jaberi, F.A., 1998. Temperature fluctuations in particle-laden homogeneous turbulent flows. Int. J. Heat Mass Transfer 41 (24), 4081–4093.

Kennedy, C.A., Carpenter, M.H., 1994. Several new numerical methods for compressible shear-layer simulations. Appl. Num. Math. 14, 397–433.

Lazaro, B.J., Lasheras, J.C., 1989. Particle dispersion in a turbulent, plane, free shear layer. Phys. Fluids A 1 (6), 1035–1044.

Ling, W., Chung, J.N., Troutt, T.R., Crowe, C.T., 1998. Direct numerical simulation of a three-dimensional temporal mixing layer with particle dispersion. J. Fluid Mech. 358, 61–85.

Lisin, F.N., Hetsroni, G., 1995. Spectrum of temperature fluctuations in high-temperature turbulent gas-particle flow. Int. J. Heat Mass Transfer 38 (4), 723–730.

Longmire, E.K., Eaton, J.K., 1992. Structure of a particle-laden round jet. J. Fluid Mech. 236, 217–257.

Mashayek, F., 1998. Droplet-turbulence interactions in low-Mach-number homogeneous shear two-phase flows. J. Fluid Mech. 367, 163–203.

Mashayek, F., Jaberi, F.A., Miller, R.S., Givi, P., 1997. Dispersion and polydispersity of droplets in stationary isotropic turbulence. Int. J. Multiphase Flow 23 (2), 337–355.

Maxey, M.R., Riley, J.J., 1983. Equation of motion for a small rigid sphere in a nonuniform flow. Phys. Fluids 26 (4), 883–889.

Mei, R., 1992. An approximate expression for the shear lift force on a spherical particle at finite Reynolds number. Int. J. Multiphase Flow 18 (1), 145–147.

Menon, S., Pannala, S. 1997. Subgrid modeling of unsteady two-phase turbulent flows. AIAA Paper 97-3113.

Miller, R.S., Bellan, J., 1999. Direct numerical simulation of a confined three-dimensional gas mixing layer with one evaporating hydrocarbon-droplet laden stream, J. Fluid Mech. in press.

Odar, F., Hamilton, W.S., 1964. Forces on a sphere accelerating in a viscous fluid. J. Fluid Mech. 18, 302–314.

Pannala, S., Menon, S. 1998. Large eddy simulations of two-phase turbulent flows. AIAA Paper 98-0163.

Saffman, P.G., 1965. The lift on a small sphere in a slow shear flow. J. Fluid Mech. 22, 385–400.

Saffman, P.G., 1968. Corrigendum to 'the lift on a small sphere in a slow shear flow'. J. Fluid Mech. 31, 624.

Shirolkar, J.S., Coimbra, C.F.M., McQuay, M.Q., 1996. Fundamental aspects of modeling turbulent particle dispersion in dilute flows. Prog. Energy Combust. Sci. 22, 363–399.

Simonin, O., Deutsch, E., Boivin, M., 1995. Large eddy simulation and second-order moment closure model of particle fluctuating motion in two-phase turbulent shear flows. In: Durst, F., Kasagi, N., Launder, B. (Eds.), Turbulent Shear Flows 9, p. 85.

Squires, K.D., Eaton, J.K., 1991. Measurements of particle dispersion obtained from direct numerical simulations of isotropic turbulence. J. Fluid Mech. 226, 1–35.

Swanson, T.R., Richards, C.D., 1997. The structure of an acoustically-forced droplet-laden jet. Atomization and Sprays 7, 561–579.

Uijttewaal, W.S.J., Oliemans, R.V.A., 1996. Particle dispersion and deposition in direct numerical and large eddy simulations of vertical pipe flow. Phys. Fluids 8 (10), 2590–2604.

Uthuppan, J., Aggarwal, S.K., Grinstein, F.F., Kailasanath, K., 1994. Particle dispersion in a transitional axisymmetric jet: a numerical simulation. AIAA J. 32 (10), 2004–2014.

Vojir, D.J., Michaelides, E.E., 1994. Effect of the history term on the motion of rigid spheres in a viscous fluid. Int. J. Multiphase Flow 20 (3), 547–556.

Wang, Q., Squires, K.D., 1996a. Large eddy simulation of particle deposition in a vertical turbulent channel flow. Int. J. Multiphase Flow 22 (4), 667–683.

Wang, Q., Squires, K.D., 1996b. Large eddy simulation of particle-laden turbulent channel flow. Phys. Fluids 8 (5), 1207–1223.

Wang, Q., Squires, K.D. 1996c. Large eddy simulations of particle dispersion in a three-dimensional turbulent mixing layer. The Fluids Engineering Division Conference, FED 236. ASME. pp. 33–40.

Wang, Q., Squires, K.D., 1998. Transport of heavy particles in a three-dimensional mixing layer. Journal of Fluids Engineering 120, 613–620.

Wang, Q., Squires, K.D., Chen, M., McLaughlin, J.B., 1997. On the role of the lift force in turbulence simulations of particle deposition. Int. J. Multiphase Flow 23 (4), 749–763.

Ye, J., Richards, C.D., 1996. Droplet and vapor transport in a turbulent jet. In: Proceedings of the 26th International Symposium on Combustion. The Combustion Institute, Pittsburg, PA, pp. 1679–1685.

Ye, J., Swanson, T.R., Richards, C.D., 1995. Particle transport and dispersion in the near field of a turbulent jet. In: Proceedings of the 1995 ASME/JSME Fluids Engineering and Laser Anemometry Conference and Exhibition, FED 228. ASME, pp. 89–94.

Zhou, L., 1993. Theory and Numerical Modeling of Turbulent Gas-Particle Flows and Combustion. CRC Press, Beijing, China.